A. Peter Allan
Miles A. Townsend
Department of Mechanical, Aerospace, and Nuclear Engineering
University of Virginia
Charlottesville, VA 22901

Motions of a Constrained Spherical Pendulum in an Arbitrarily Moving Reference Frame: The Automobile Seatbelt Inertial Sensor

A common automatic seatbelt inertial sensor design, comprised of a constrained spherical pendulum, is modeled to study its motions and possible unintentional release during vehicle emergency maneuvers. The kinematics are derived for the system with the most general inputs: arbitrary pivot motions. The influence of forces due to gravity and constraint torque functions is developed. The equations of motion are then derived using Kane's method. The equations of motion are used in a numerical simulation with both actual and hypothetical automobile crash data. © *1995 John Wiley & Sons, Inc.*

INTRODUCTION

This article addresses the motions of a spherical pendulum in a gravitational field in response to arbitrary motions of its pivot point. The motivation is the widespread application of the spherical pendulum as an inertial sensor in automobile seatbelt retractor mechanisms, as shown in Figure 1. The belt locking mechanism is activated by the pendulum's polar angle relative to the vehicle (q_2) to prevent the unreeling of the seatbelt during rapid deceleration or overturning. Each seatbelt has such a mechanism.

The equations of motion are formed using Kane's equations, a form of Newton's equations, in which nonworking forces of constraint are "automatically" eliminated; accordingly, the analysis considers only the actual degrees of freedom. Numerical simulation of these equations for actual and hypothetical inputs is used to predict conditions under which the retractor mechanism might fail to lock or be unlocked, for example due to rebound, oscillations of the pendulum, or motions of the vehicle.

SPECIFICATION OF SYSTEM

The points, reference frames, and coordinates are shown in Figure 2. An inertial frame **A** is fixed at some convenient point on the earth. The vehicle is characterized by a reference point *B*

Received September 30, 1994; Accepted December 8, 1994.

Shock and Vibration, Vol. 2, No. 3, pp. 227–236 (1995)

CCC 1070-9622/95/030227-10

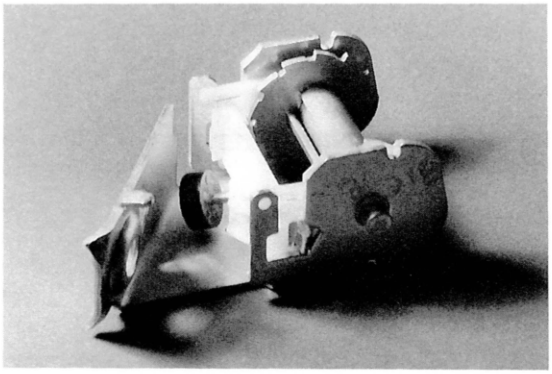

FIGURE 1

and frame **B** with unit vectors $\mathbf{b}_i$, per Figure 2(a). The pivot point of a pendulum is at P_1 located at $\mathbf{r}^{BP_1}$ in the **B** frame. The pendulum is assumed to be a mass m on a rigid rod of length L at point P_2 in Figure 2(b). (A distributed-mass pendulum could be assumed, but no generality is gained.)

The translational velocity of point B and angular velocity of the vehicle frame **B** relative to **A** are given by

$$\mathbf{v} \equiv {}^A\mathbf{v}^B = v_1\mathbf{b}_1 + v_2\mathbf{b}_2 + v_3\mathbf{b}_3 \tag{1}$$

$$\omega \equiv {}^A\omega^B = \Omega_1\mathbf{b}_1 + \Omega_2\mathbf{b}_2 + \Omega_3\mathbf{b}_3, \tag{2}$$

respectively. These are specified inputs to the system, i.e., v_i and Ω_i are given functions of time or can be calculated from the initial position and orientation as follows. The orientation of the vehicle in **A** is specified by three orientation angles: starting with the **B** and **A** systems aligned, **B** is rotated through ψ about the "vertical" $\mathbf{a}_3 - \mathbf{b}_3$ axis, followed by a rotation θ about the "new" $\mathbf{b}_2$ axis, and finally a rotation ϕ about this latest $\mathbf{b}_1$ axis. These correspond to the motions of yaw, pitch, and roll of the vehicle. Accordingly, the orientation of **B** relative to **A** (and the componentiation of any vector in **B**) is given by the resulting orthogonal direction cosine matrix ${}^BC^A$

$$\begin{bmatrix}\mathbf{b}_1\\ \mathbf{b}_2\\ \mathbf{b}_3\end{bmatrix} = [{}^BC^A]\begin{bmatrix}\mathbf{a}_1\\ \mathbf{a}_2\\ \mathbf{a}_3\end{bmatrix} \tag{3}$$

where

$$[{}^BC^A] = \begin{bmatrix} c_\psi c_\theta & s_\psi c_\theta & -s_\theta \\ (-s_\psi c_\phi + c_\psi s_\theta s_\phi) & (c_\psi c_\phi + s_\psi s_\theta s_\phi) & c_\theta s_\phi \\ (s_\psi s_\phi + c_\psi s_\theta c_\phi) & (-c_\psi s_\phi + s_\psi s_\theta c_\phi) & c_\theta c_\phi \end{bmatrix}. \tag{4}$$

The notation is $c_\psi = \cos\psi$, $s_\psi = \sin\psi$, etc. The relation between the Ω_i in Eq. (2) and these orientation angles and their time derivatives is

$$\begin{bmatrix}\Omega_1\\ \Omega_2\\ \Omega_3\end{bmatrix} = \begin{bmatrix} -s_\theta & 0 & 1 \\ c_\theta s_\phi & c_\phi & 0 \\ c_\theta c_\phi & -s_\phi & 0 \end{bmatrix}\frac{d}{dt}\begin{bmatrix}\psi\\ \theta\\ \phi\end{bmatrix}. \tag{5}$$

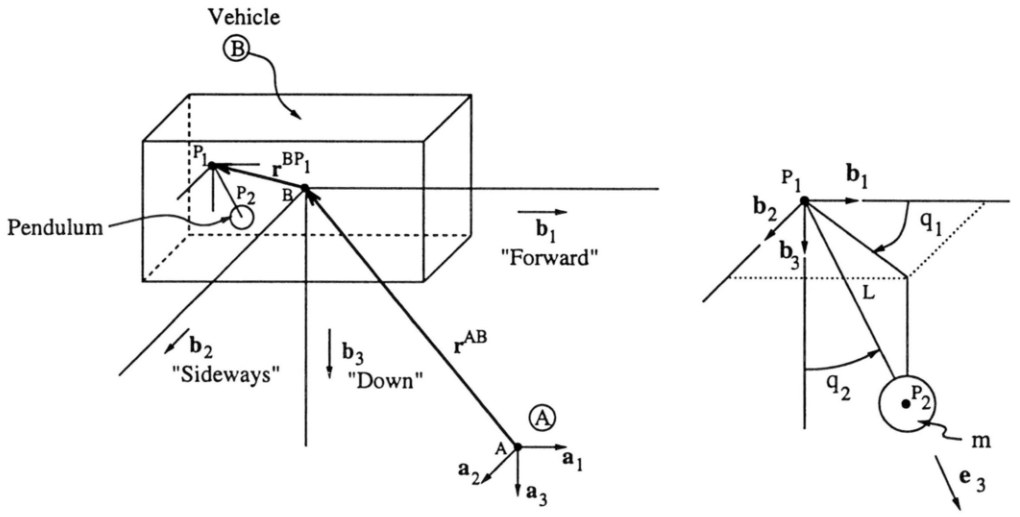

(a) Vehicle System

(b) Detail of pendulum

FIGURE 2

Derivations of Eqs. (3)–(5) are available in the literature, e.g., Junkins and Turner (1986).

The velocity and acceleration of P_1 are:

$$ {}^{A}\mathbf{v}^{P_1} = \mathbf{v} + \omega \times \mathbf{r}^{BP_1} \tag{6} $$

$$ {}^{A}\mathbf{a}^{P_1} = \frac{{}^{A}d}{dt}\mathbf{v} + \dot{\omega} \times \mathbf{r}^{BP_1} + \omega \times (\omega \times \mathbf{r}^{BP_1}). \tag{7} $$

These are known functions of time from the system geometry and specified inputs, as follows. The first term in Eq. (7) is

$$ \frac{{}^{A}d}{dt}\mathbf{v} = \frac{{}^{B}d}{dt}\mathbf{v} + \omega \times \mathbf{v} = {}^{B}\mathbf{a}^{B} + \omega \times \mathbf{v} \tag{8} $$

where ${}^{B}\mathbf{a}^{B}$ is the time derivatives of the v_i in Eq. (1). The angular acceleration $\dot{\omega}$ in Eq. (7) is composed of the time derivatives of the Ω_i in Eq. (2). Thus, everything needed to calculate the acceleration of P_1 as a function of time is given by the geometry and specified input motions.

KINEMATICS OF THE PENDULUM

The pendulum variables are the azimuthal and polar angles relative to the **B** frame, q_1 and q_2, respectively, in Figure 2(b). Introduction of a frame **E** fixed in the pendulum is useful; **E** is related to **B** by direction cosine matrix ${}^{E}C^{B}$

$$ \begin{bmatrix} \mathbf{e}_1 \\ \mathbf{e}_2 \\ \mathbf{e}_3 \end{bmatrix} = [{}^{E}C^{B}] \begin{bmatrix} \mathbf{b}_1 \\ \mathbf{b}_2 \\ \mathbf{b}_3 \end{bmatrix} = \begin{bmatrix} c_2c_1 & c_2s_1 & -s_2 \\ -s_1 & c_1 & 0 \\ s_2c_1 & s_2s_1 & c_2 \end{bmatrix} \begin{bmatrix} \mathbf{b}_1 \\ \mathbf{b}_2 \\ \mathbf{b}_3 \end{bmatrix} \tag{9} $$

where $c_2 = \cos q_2$, etc. Accordingly, the pendulum is described by

$$ \mathbf{r}^{P_1P_2} = L\mathbf{e}_3 = L(s_2c_1\mathbf{b}_1 + s_2s_1\mathbf{b}_2 + c_2\mathbf{b}_3). \tag{10} $$

The angular velocity of the pendulum **E** relative to **B** is variously [from Fig. 2(b)]

$$ \begin{aligned} {}^{B}\omega^{E} &= \dot{q}_1\mathbf{b}_3 + \dot{q}_2\mathbf{e}_2 \\ &= \mathbf{b}_3q_1 + (c_1\mathbf{b}_2 - s_1\mathbf{b}_1)\dot{q}_2 \\ &= (-s_2\mathbf{e}_1 + c_2\mathbf{e}_3)\dot{q}_1 + \mathbf{e}_2\dot{q}_2. \end{aligned} \tag{11} $$

The velocity of P_2 in **A** is

$$ {}^{A}\mathbf{v}^{P_2} = {}^{A}\mathbf{v}^{P_1} + \frac{{}^{B}d}{dt}\mathbf{r}^{P_1P_2} + \omega \times \mathbf{r}^{P_1P_2}. \tag{12} $$

In Eq. (12) ${}^{A}\mathbf{v}^{P_1}$ is from the known inputs, Eq. (6). The latter two terms give the velocity of P_2 relative to P_1 in **A**. The second term is the time derivative of $\mathbf{r}^{P_1P_2}$ in **B**; from Eq. (10):

$$ \begin{aligned} {}^{B}\dot{\mathbf{r}}^{P_1P_2} &= L\{(c_2c_1\mathbf{b}_1 + c_2s_1\mathbf{b}_2 - s_2\mathbf{b}_3)\dot{q}_2 \\ &\quad + s_2(-s_1\mathbf{b}_1 + c_1\mathbf{b}_2)\dot{q}_1\} \\ &= L(\mathbf{e}_1\dot{q}_2 + s_2\mathbf{e}_2\dot{q}_1). \end{aligned} \tag{13} $$

The third term of Eq. (12) is found using Eqs. (2) and (10).

The absolute acceleration of P_2 is

$$ {}^{A}\mathbf{a}^{P_2} = {}^{A}\mathbf{a}^{P_1} + \frac{{}^{A}d}{dt}{}^{B}\dot{\mathbf{r}}^{P_1P_2} + \frac{{}^{A}d}{dt}(\omega \times \mathbf{r}^{P_1P_2}) \tag{14} $$

$$ \begin{aligned} &= {}^{A}\mathbf{a}^{P_1} + \dot{\omega} \times \mathbf{r}^{P_1P_2} + \omega \times (\omega \times \mathbf{r}^{P_1P_2}) \\ &\quad + 2\omega \times {}^{B}\dot{\mathbf{r}}^{P_1P_2} + {}^{B}\ddot{\mathbf{r}}^{P_1P_2}. \end{aligned} \tag{15} $$

The acceleration of P_1 is from the inputs, per Eqs. (4) and (5). Terms 2, 3, and 4 in Eq. (15) can be calculated using Eqs. (2), (6), and (9). The last term in Eq. (15) can be evaluated by differentiating Eq. (10) in the **B** frame, but it is more convenient to do it in the **E** frame using Eqs. (10), (11), and (13):

$$ {}^{B}\ddot{\mathbf{r}}^{P_1P_2} = \frac{{}^{E}d}{dt}{}^{B}\dot{\mathbf{r}}^{P_1P_2} + {}^{B}\omega^{E} \times {}^{B}\dot{\mathbf{r}}^{P_1P_2} \tag{16} $$

$$ \begin{aligned} &= L\{(\ddot{q}_2 - s_2c_2\dot{q}_1^2)\mathbf{e}_1 \\ &\quad + (s_2\ddot{q}_1 + 2c_2\dot{q}_1\dot{q}_2)\mathbf{e}_2 - (\dot{q}_2^2 + s_2^2\dot{q}_1^2)\mathbf{e}_3\}. \end{aligned} \tag{17} $$

Eq. (17) can also be expressed in the **B** frame, if so desired.

This completes the kinematic analysis. The system has eight variables: three each for the translation and rotation of the vehicle, plus the two pendulum variables q_1 and q_2. Because the vehicle motions are specified, the system has only two unknown degrees of freedom, q_1 and q_2. The angle q_2 is of particular interest: it is the relative polar angle that controls the latching mechanism of Figure 1.

FORCE ANALYSIS

The forces acting on the pendulum are gravity, and elastic and damping torques at the pivot joint. The gravitational force on the pendulum bob P_2 is

$$ \mathbf{F}_2 = mg\mathbf{a}_3. \tag{18} $$

The pivot force model can incorporate the polar angle constraint, and a damping torque. The azimuthal angle is not restricted, but is subjected to a damping torque. Thus, the torque at the pivot on the pendulum **E** has two components, T_1 which damps the azimuthal angle q_1, and T_2 which both restricts (through an elastic force) and damps the polar angle q_2:

$$\begin{aligned}\mathbf{T}_E = T_1 s_2 \mathbf{b}_3 + T_2 \mathbf{e}_2 = -b_1(q_2, \dot{q}_1)s_2\mathbf{b}_3 \\ - (k(q_2) + b_2(q_2, \dot{q}_2))\mathbf{e}_2.\end{aligned} \tag{19}$$

The s_2 term is included in the expression so that the azimuthal damping torque is reduced to zero as q_2 approaches zero. The net effect of this is to give the damping torque functions equivalent effects on their respective angular rate terms in the dynamic equations Eqs. (45) and (46). T_1 and T_2 may be highly nonlinear functions to reflect constraints on the motion and the effect of the orientation of the vehicle "vertical" $\mathbf{b}_3$. Several types of constraint torque functions were explored before selecting functions of the form

$$\begin{aligned}T_1 &= -(b_0 + b_1 q_2^2 + b_2 q_2^4 + \cdots)\dot{q}_1 \\ T_2 &= -(k_0 + k_1 q_2^2 + k_2 q_2^4 + \cdots)q_2 \\ &\quad -(b_0 + b_1 q_2^2 + b_2 q_2^4 + \cdots)\dot{q}_2.\end{aligned} \tag{20}$$

These forms have several useful features. They are continuous and have continuous derivatives, which avoids problems with adaptive differential equation solvers. They provide stiffness and damping as an even function of the polar angle q_2, which is consistent with the mechanism symmetry. T_2 can be made to "turn on" as rapidly and as "hard" as desired at a specific value of q_2 to simulate the geometric constraint on q_2, by the choice and weighting of the high order terms. The high order damping terms in both T_1 and T_2 can simulate inelasticity in the collision of the pendulum shaft with the socket. The damping coefficients b_i reflect the observed decay in both variables q_1 and q_2. The same coefficients were used in both T_1 and T_2 for convenience and because no data was available to identify the azimuthal damping. Based on data available from sled crash tests, five parameters were used:

$$\begin{aligned}T_1 &= -(b_0 + b_1 q_2^2)\dot{q}_1 \\ T_2 &= -(k_0 + k_1 q_2^2 + k_4 q_2^8)q_2 - (b_0 + b_1 q_2^2)\dot{q}_2.\end{aligned} \tag{21}$$

The parameters were selected and iteratively adjusted so that the result of the simulations would closely match the pendulum behavior. The results are shown in Figure 3 and comprise case 1. The corresponding numerical values and system parameters are in Table 1.

Due to the pivot mechanism flapper (see Fig. 1), T_2 or, more likely, the spring stiffness or force, may also be a function of the orientation of the vehicle "down" $\mathbf{b}_3$ relative to the fixed gravity field vertical $\mathbf{a}_3$ such that the restraining force would decrease if the vehicle rolls over. This is given by $\mathbf{b}_3 \cdot \mathbf{a}_3$, the c_{33} component of $[^B C^A]$, which is $c_\theta c_\phi$ per Eq. (4). For example, if the stiffness function is simply related to the orientation, the relation might be

$$k(q_2, \mathbf{b}_3) = \tfrac{1}{2}(1 + c_\theta c_\phi)k(q_2). \tag{22}$$

The function varies between 1 and 0: 1 when $\mathbf{b}_3$ and $\mathbf{a}_3$ are aligned and 0 when opposed due to either θ or ϕ. The dependence of the stiffness on

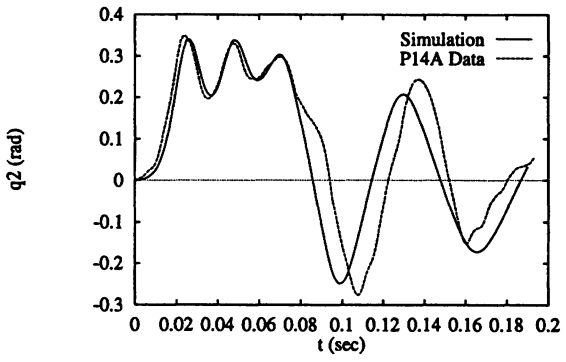

(a) Polar Angle vs. Time.

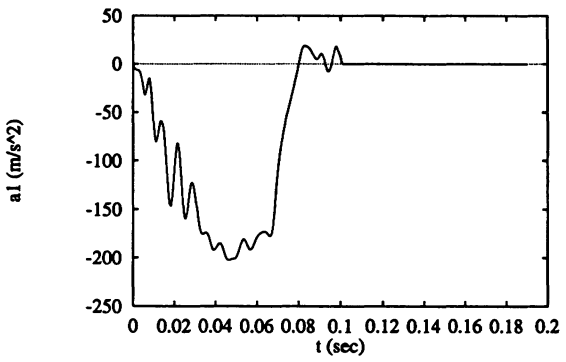

(b) Acceleration vs. Time.

FIGURE 3

Table 1. Model Parameters

Parameter	Symbol	Guess	Value	Unit
Constraint torques	k_0	0.0156	0.0172	Nm/rad
	k_1	5.85	5.62	Nm/rad^3
	k_4	1100	910	Nm/rad^9
	b_0	0.000279	0.000201	Nm/rad s
	b_1	0.00459	0.0127	Nm/rad^3 s
Pendulum arm length	l	0.0191	0.0263	m
Pendulum mass	m		0.0320	kg
Pendulum location	r_1		−0.737	m
	r_2		0.706	m
	r_3		0.0584	m

q_2 is retained. Due to a lack of available calibration data, this effect was ignored in simulations.

EQUATIONS OF MOTION

Kane's equations of motion address only the salient degrees of freedom and suppresses nonworking constraint forces. This methodology entails defining the so-called generalized speeds and partial velocities and then forming generalized active and inertial forces corresponding to the generalized speeds.

The generalized speeds are linear functions of the time derivatives of the generalized coordinates; here, they are selected as

$$u_1 = \dot{q}_1, \quad u_2 = \dot{q}_2. \tag{23}$$

This choice is not particularly imaginative; however, these speeds are physically significant because they correspond to the generalized and actual coordinates of interest. This choice also simplifies checks with other formulations.

The partial velocities are the coefficients of the generalized speeds in the velocity equations for P_1 and P_2. In Eqs. (6), (12), and (13) the generalized speeds appear only in the P_1P_2 term [Eq. (13)] and are

$$\begin{aligned} \mathbf{v}_1^{P_1} &= \mathbf{v}_2^{P_1} = 0 \\ \mathbf{v}_1^{P_2} &= Ls_2\mathbf{e}_2 = Ls_2(-s_1\mathbf{b}_1 + c_1\mathbf{b}_2) \\ \mathbf{v}_2^{P_2} &= L\mathbf{e}_1 = L(c_2c_1\mathbf{b}_1 + c_2s_1\mathbf{b}_2 - s_2\mathbf{b}_3). \end{aligned} \tag{24}$$

The superscripts refer to the respective points of interest, P_1 and P_2; the subscripts refer to the generalized speeds u_1 and u_2. The remaining terms in the velocities of P_1 and P_2 are established by the independent inputs.

Similarly, the partial angular velocities are the coefficients of the generalized speeds, and these appear only in the ${}^B\omega^E$ term in Eq. (11). It turns out that the **E** frame expressions are more convenient:

$$\begin{aligned} \omega_1^E &= -s_2\mathbf{e}_1 + c_2\mathbf{e}_3 \\ \omega_2^E &= \mathbf{e}_2 \end{aligned} \tag{25}$$

Kane's equations are expressed in terms of generalized active forces and generalized inertial forces:

$$Q_r + Q_r^* = 0, \quad r = 1, \ldots, n. \tag{26}$$

n is the number of generalized speeds (2 here).

The rth generalized active force is given by

$$Q_r = \sum_{j=1}^{J} \mathbf{v}_r^{P_j} \cdot \mathbf{F}_j, \quad r = 1, \ldots, n. \tag{27}$$

$\mathbf{F}_j$ is the sum of the forces acting at the point P_j. The generalized force due to the pivot point spring and damper is

$$(Q_r)_E = \omega_r^E \cdot \mathbf{T}_E. \tag{28}$$

$\mathbf{T}_E$ is from Eqs. (19) and (21).

The rth generalized inertia force is

$$Q_r^* = \sum_{i=1}^{p} \mathbf{v}_r^{P_i} \cdot (-m_i{}^A\mathbf{a}^{P_i}), \quad r = 1, \ldots, n. \tag{29}$$

There are p masses in the system. The points in Eq. (29) may be different than in Eq. (27).

The pendulum can also be considered as a rigid body, in which case the generalized active forces are evaluated as:

$$(Q_r)_E = \omega_r^E \cdot \mathbf{T}_E + \mathbf{v}_r^{P_k} \cdot \mathbf{F}_k \tag{30}$$

where $\mathbf{T}_E$ and $\mathbf{F}_k$ are the moments and forces resolved about some point k. (Here, k would surely be P_2.) The generalized inertia forces with respect to the pendulum center of mass (E^*) are:

$$(Q_r^*)_E = \omega_r^E \cdot \mathbf{T}_E^* + \mathbf{v}_r^{E^*} \cdot (-M\mathbf{a}^{E^*}) \tag{31}$$

where

$$\mathbf{T}_E^* = -{}^B\dot{\omega}^E \cdot \underline{\mathbf{I}}^* - \omega \times \underline{\mathbf{I}}^* \cdot \omega. \tag{32}$$

$\underline{\mathbf{I}}^*$ is the central inertia dyadic of the body.

For this case of a point mass pendulum, we can use either group of equations, i.e., Eqs. (27)–(29) or Eqs. (30)–(32) or some convenient combination, so long as no duplication occurs. In the latter case, the moments of inertia of the point pendulum with respect to its center of mass at E^* are zero.

GENERAL SOLUTION

The generalized active forces corresponding to Eq. (30) are:

$$Q_1 = -s_2 T_1 + mgLs_2(\mathbf{e}_2 \cdot \mathbf{a}_3) \tag{33}$$

$$Q_2 = T_2 + mgL(\mathbf{e}_1 \cdot \mathbf{a}_3). \tag{34}$$

The torque functions T_1 and T_2 are from Eqs. (21). The direction cosines are calculated from the c_{23} and c_{13} elements of

$$[{}^EC^A] = [{}^EC^B][{}^BC^A]. \tag{35}$$

From Eqs. (4) and (9) these are

$$\begin{aligned} \mathbf{e}_2 \cdot \mathbf{a}_3 &= s_1 s_\theta + c_1 c_\theta s_\phi \\ \mathbf{e}_1 \cdot \mathbf{a}_3 &= -c_2 c_1 s_\theta + c_2 s_1 c_\theta s_\phi - s_2 c_\theta c_\phi. \end{aligned} \tag{36}$$

The accelerations for the generalized inertia forces are given by Eqs. (14)–(17), and the trivial substitution for the generalized speeds of Eq. (23) and their derivatives. In the following, the equations of motion are presented explicitly, although they can easily be calculated algorithmically as indicated earlier.

The acceleration of P_1 is not needed independently because the associated partial velocities are zero. (This is physically and intuitively obvious; the "mass" at P_1 is zero.) Because of the assumed specification of the vehicle motions, it is convenient to rewrite the acceleration of P_2 in Eq. (15) as

$$\begin{aligned} {}^A\mathbf{a}^{P_2} = {}^A\mathbf{a}^B &+ \dot{\omega} \times (\mathbf{r}^{BP_1} + \mathbf{r}^{P_1P_2}) \\ &+ \omega \times (\omega \times (\mathbf{r}^{BP_1} + \mathbf{r}^{P_1P_2})) \\ &+ 2\omega \times {}^B\dot{\mathbf{r}}^{P_1P_2} + {}^B\ddot{\mathbf{r}}^{P_1P_2}. \end{aligned} \tag{37}$$

Performing the operations indicated, Eq. (37) can be written

$$\begin{aligned} {}^A\mathbf{a}^{P_2} = Z_1\mathbf{b}_1 + Z_2\mathbf{b}_2 + Z_3\mathbf{b}_3 + 2\omega \\ \times {}^B\dot{\mathbf{r}}^{P_1P_2} + {}^B\ddot{\mathbf{r}}^{P_1P_2}. \end{aligned} \tag{38}$$

The Z_i, $i = 1, 2, 3$ are functions of the given parameters, inputs, and q_1 and q_2. Specifically,

$$\begin{aligned} Z_1 = \dot{v}_1 &+ v_3\Omega_2 - v_2\Omega_3 + (r_3 + Lc_2)\dot{\Omega}_2 \\ &- (r_2 + Ls_2s_1)\dot{\Omega}_3 \\ &- (r_1 + Ls_2c_1)(\Omega_2^2 + \Omega_3^2) \\ &+ (r_2 + Ls_2s_1)\Omega_1\Omega_2 + (r_3 + Lc_2)\Omega_1\Omega_2 \end{aligned} \tag{39}$$

$$\begin{aligned} Z_2 = \dot{v}_2 &+ v_1\Omega_3 - v_3\Omega_1 - (r_3 + Lc_2)\dot{\Omega}_1 \\ &+ (r_1 + Ls_2c_1)\dot{\Omega}_3 \\ &- (r_2 + Ls_2s_1)(\Omega_1^2 + \Omega_3^2) \\ &+ (r_1 + Ls_2c_1)\Omega_1\Omega_2 + (r_3 + Lc_2)\Omega_2\Omega_3 \end{aligned} \tag{40}$$

$$\begin{aligned} Z_3 = \dot{v}_3 &+ v_2\Omega_1 - v_1\Omega_2 + (r_2 + Ls_2s_1) \\ &+ \dot{\Omega}_1 - (r_1 + Ls_2c_1)\dot{\Omega}_2 \\ &- (r_3 + Lc_2)(\Omega_1^2 + \Omega_2^2) \\ &+ (r_1 + Ls_2c_1)\Omega_1\Omega_3 + (r_2 + Ls_2s_1)\Omega_2\Omega_3 \end{aligned} \tag{41}$$

where $\mathbf{r}^{BP_1} = r_1\mathbf{b}_1 + r_2\mathbf{b}_2 + r_3\mathbf{b}_3$. The Coriolis acceleration in Eqs. (37) and (38) is written as

$$2\omega \times {}^B\dot{\mathbf{r}}^{P_1P_2} = Z_4\mathbf{b}_1 + Z_5\mathbf{b}_2 + Z_6\mathbf{b}_3 \tag{42}$$

where

$$\begin{aligned} Z_4 &= 2L[s_2u_2\Omega_2 - (c_2s_1u_2 + s_2c_1u_1)\Omega_3] \\ Z_5 &= 2L[-s_2u_2\Omega_1 + (c_1c_2u_2 - s_2s_1u_1)\Omega_3] \\ Z_6 &= 2L[(c_2s_1u_2 + s_2c_1u_1)\Omega_1 \\ &\quad - (c_1c_2u_2 - s_2s_1u_1)\Omega_2]. \end{aligned} \tag{43}$$

With Eq. (17), the generalized inertia forces are the negative of

$$
\begin{aligned}
m^A\mathbf{a}^{P_2} \cdot \mathbf{v}_r^{P_2} = mL\{&(\dot{u}_2 - s_2c_2u_1^2)\mathbf{e}_1 \\
&+ (s_2\dot{u}_1 + 2c_2u_1u_2)\mathbf{e}_2 \\
&+ (-u_2^2 - s_2^2u_1^2)\mathbf{e}_3\} \cdot \mathbf{v}_r^{P_2}(\underline{\mathbf{e}}) \\
&+ m\{(Z_1 + Z_4)\mathbf{b}_1 + (Z_2 + Z_5)\mathbf{b}_5 \\
&+ (Z_3 + Z_6)\mathbf{b}_3\} \cdot \mathbf{v}_r^{P_2}(\underline{\mathbf{b}})
\end{aligned}
\tag{44}
$$

for $r = 1, 2$. The $\mathbf{v}_r(\underline{\mathbf{e}})$ and $\mathbf{v}_r(\underline{\mathbf{b}})$ indicate componentiation in the respective frames, per Eq. (25). This form is very easy to use.

The results of Eq. (44) and Eqs. (33) and (34) are substituted into Eq. (26) and rearranged to yield the dynamic equations:

$$
\begin{aligned}
Ls_2\dot{u}_1 = &-2Lc_2u_1u_2 + s_1(Z_1 + Z_4) - c_1(Z_2 + Z_5) \\
&+ g(s_1s_\theta + c_1c_\theta s_\phi) + \frac{T_1s_2}{mL}
\end{aligned}
\tag{45}
$$

$$
\begin{aligned}
L\dot{u}_2 = &\; Ls_2c_2u_1^2 - c_2c_1(Z_1 + Z_4) \\
&- c_2s_1(Z_2 + Z_5) + s_2(Z_3 + Z_6) \\
&+ g(-c_2c_1s_\theta + c_2s_1c_\theta s_\phi \\
&- s_2\,c_\theta c_\phi) + \frac{T_2}{mL}.
\end{aligned}
\tag{46}
$$

Eqs. (45) and (46) are supplemented by the definitions of the generalized speeds of Eq. (23) and the orientation (Euler) angles rate equations for ψ, θ, and ϕ in Eq. (5). These are seven first-order ordinary differential equations to be integrated in time to give the orientation of the vehicle and the pendulum position in the vehicle. The only real unknowns are the q_i and u_i. The velocity of the vehicle and the vehicle displacement (in the earth frame) are straightforward integration and transformations of the given inputs, once the orientation angles are calculated.

The solution requires as inputs:

- system parameters:
  —location of P_1 in the vehicle: r_1, r_2, r_3
  —*pendulum parameters*: L, m, g; pivot torque functions T_1, T_2;
- vehicle motions as functions of time:
  —velocity components of the vehicle and their time derivatives: v_1, v_2, v_3, $\dot{v}_1$, $\dot{v}_2$, $\dot{v}_3$
  —angular velocity components of the vehicle and their time derivatives: Ω_1, Ω_2, Ω_3, $\dot{\Omega}_1$, $\dot{\Omega}_2$, $\dot{\Omega}_3$;
- initial conditions not specified by the vehicle motions, i.e., q_1, q_2, u_1, u_2. Normally these will be zero.

SIMULATION

The dynamics of the system, specified by Eqs. (5), (23), (45), and (46) were solved numerically for three cases. Case 1 employs actual crash data to both validate the model and establish parameters for the pendulum constraint torque model of Eqs. (20) and (21). Regression methods were used with this data to determine model parameters. Case 2 adds a side impact to case 1. Case 3 investigates pendulum behavior in an airborne accident scenario.

Case 1

Data was obtained from the University of Virginia Automobile Safety Lab from a seatbelt retractor pendulum mounted in a vehicle on a sled that was collided with a hard stop while traveling at 22.2 mph. The data comprise a pendulum polar angle trace (digitized from 1000 frame/second film) shown as the dashed trace of Figure 1(a) and an acceleration pulse from an accelerometer shown in Figure 1(b). Both data sets are indexed to $t = 0$ at the start of the impact.

The acceleration pulse was used as input to the model as $\dot{v}_1$. All other inputs were held zero (v_1 is not zero in reality, but it is always multiplied by some Ω_i in the dynamic equations, all of which are zero for this maneuver, so is irrelevant). The parameters k_0, k_1, k_4, b_0, and b_1 were adjusted so that the result of the simulation would closely match the data as shown in Figure 3(a). It can be seen in Figure 3 that the pivot remains in the belt locking position ($q_2 > 0.15$ rad estimated) for almost all of the impact, and that when it is not in the locking position (near $t = 0.08$ s) the mechanism will not unlock due to continued tension on the belt.

The initial parameter adjustments sought to provide a starting point such that an automated regression scheme would yield feasible, i.e., nonnegative, results.

The regression used the nonlinear simplex method to minimize the cost function

$$
C = 10\int_{t=0}^{t=0.08}(q_2 - \bar{q}_2)^2\,dt + \int_{t=0.08}^{t=0.14}(q_2 - \bar{q}_2)^2\,dt \tag{47}
$$

in the space of parameters. Because the measurement of the length of the pendulum arm l was imprecise, it was added to the set of free parameters.

This regression method was subject to overfitting certain regions of the curve, while missing other important regions. The weights and limits of integration needed frequent adjustments, and the process had to be interrupted before converging at times. (This is the reason for the initial adjustment phase.) It was however helpful in getting a close fit. The final parameters established for the model are shown in Table 1 together with the best guess before regression. These appear to be reasonable values, e.g., all are positive and within "eyeball" limits.

NUMERICAL CONSIDERATIONS

Case 1, discussed in the previous section, was solved using two different but equivalent methods. *Mathematica*, as described in Wolfram (1988), was used to get a model working quickly due to its terse syntax. A *C* language code was written using the *ODEPACK* solvers, as described in Hindmarsh (1983), and verified to give the same results as the *Mathematica* code. The *C* code runs substantially faster, and thus cases 2 and 3 were run with it only.

Both solutions use a heuristic that switches between stiff and nonstiff solution methods. The estimated step size at the current state of the equations is the basis for the decision. This scheme is described in Petzold (1983). In the stiff case the Adams predictor-corrector method is used, and in the nonstiff case the backward difference, or Gear, method is used.

For a one degree-of-freedom problem, such as simulating a head-on collision, the equations simplify dramatically, and solutions were completed quickly (about 3 CPU s on an IBM RS/6000). When, however, the full six degree-of-freedom problem was solved, solutions took several

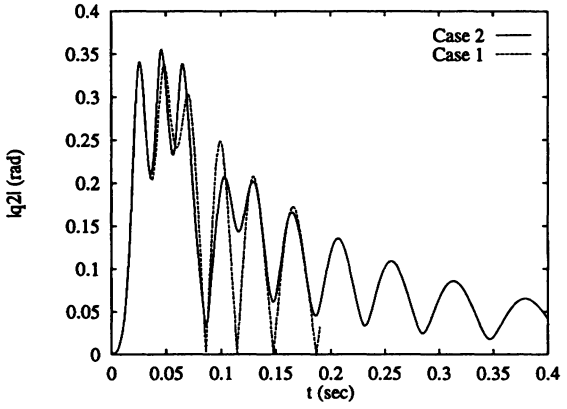

(a) Polar Angle vs. Time.

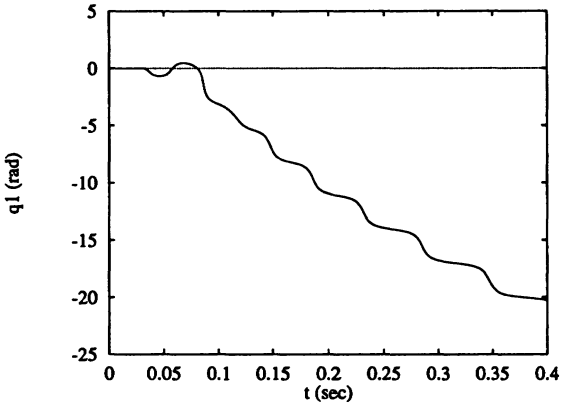

(b) Azimuthal Angle vs. Time.

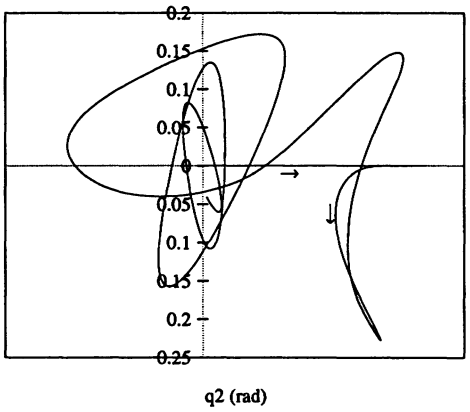

(c) Polar Plot of Polar Angle vs. Azimuthal Angle.

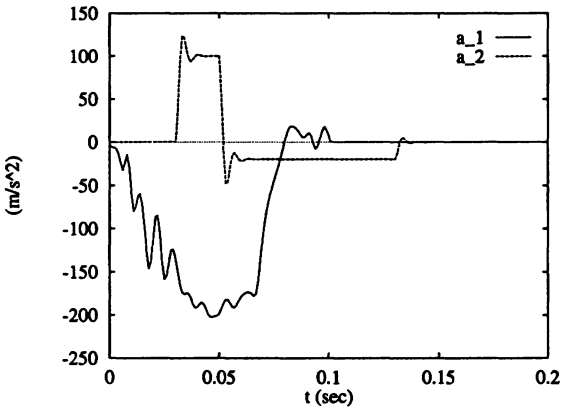

(d) Accelerations vs. Time (input)

FIGURE 4

hours. Although *Mathematica* uses some internal compilation of the code, it is largely an interpreted language, which makes it inherently slow for large computational tasks. The *C* code solved the one degree-of-freedom cases in about 0.4 CPU and the six degree-of-freedom cases in about 2.8 CPU s. This speed allowed regression to be used for model parameter determination. Regression used the nonlinear simplex method described by Press et al. (1989).

Case 2

This case extends case 1 by adding a hypothetical side impact after the start of the original head-on collision. The inputs are shown in Figure 4(d). The initial motion is longitudinal, along the horizontal axis in Figure 4(c), and then goes into a whirl after the side impact as shown by the arrows. Other than the whirl, the polar angle is quite similar to case 1 as shown in Figure 4(a). The possibility of unlocking is essentially unchanged, at least during the major head-on impact.

Case 3

An accident scenario involving a vehicle that becomes airborne was explored. With some initial forward velocity and angular momentum, the vehicle continues without additional torques or forces, as described in Townsend and Allan (1994). This case tests the pendulum model in its most general sense, because all 15 inputs v_1, v_2, v_3, $\dot{v}_1$, $\dot{v}_2$, $\dot{v}_3$, Ω_1, Ω_2, Ω_3, $\dot{\Omega}_1$, $\dot{\Omega}_2$, $\dot{\Omega}_3$, θ, ϕ vary with time.

The dynamics of the vehicle were simulated independently and the results used as input. The

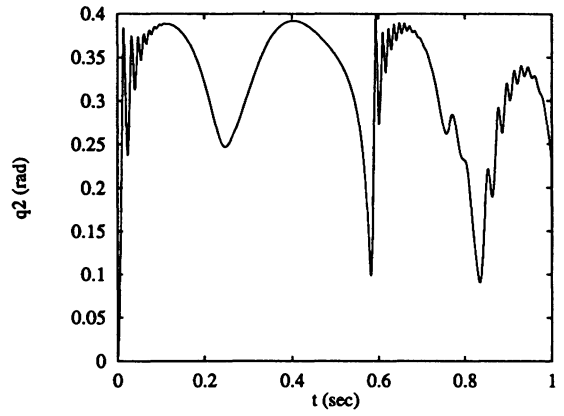

(a) Polar Angle vs. Time.

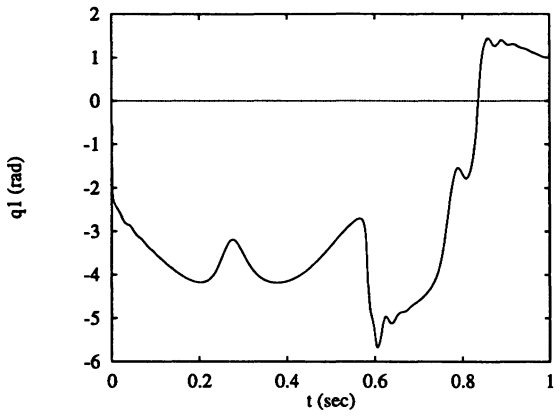

(b) Azimuthal Angle vs. Time.

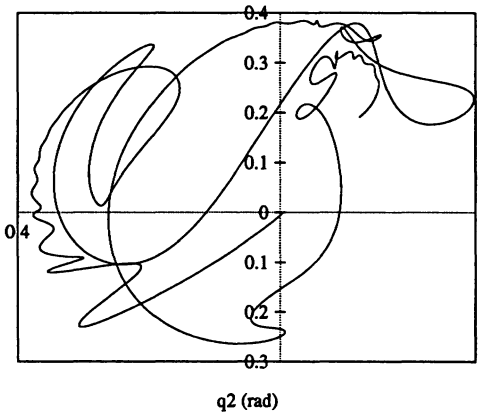

(c) Polar Plot of Polar Angle vs. Azimuthal Angle.

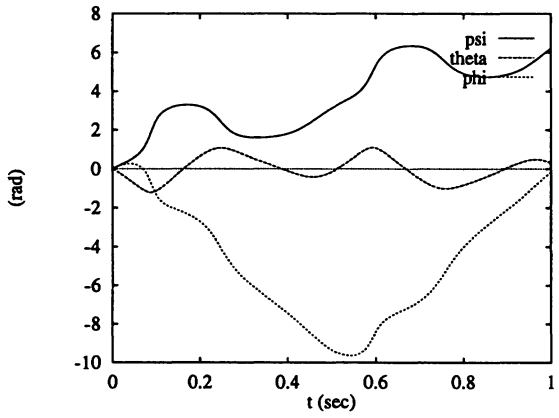

(d) Vehicle Euler Angles vs. Time (input)

FIGURE 5

initial conditions for this simulation were $v_1 = 20$ m/s, $\Omega_1 = \Omega_3 = 12$ rad/s, and $\Omega_2 = -12$ rad/s. These values were chosen to give interesting motions, and scaled to result in pendulum motions at the constraint in the range for which the model was calibrated. Note that the Euler angle ψ is an output of the vehicle dynamics, but it is not needed for the pendulum dynamics. The pendulum behavior and the vehicle's orientation are shown in Figure 5.

The simulation indicates that the pendulum attains nonlocking positions near $t = 0.6$ s and $t = 0.8$ s as can be seen in Figure 4(a). Recall that when q_2 becomes less than about 0.15 rad (and there is no tension on the belt) the toothed wheel on the retractor mechanism disengages.

Little can be said about the simulated pendulum behavior in this case relative to one's intuitive feel for how it should behave because the geometry is complex.

CONCLUSION

The complete equations of motion of a spherical pendulum have been derived for the conditions of a movable pivot point and restraining forces at that point. A pivot restraint function and its dependence on vehicle orientation have been suggested.

Two codes were developed to solve the same equations, and they give equivalent results. They are not however redundant. The *Mathematica* code is useful for development purposes, and the *C* code for quick repeated simulations.

By considering three cases, increasing in complexity, confidence is built in the reliably of the model. The model was calibrated using case 1, because it was the only one for which data was available, and a close agreement was obtained. Case 2 is similar to case 1, but a hypothetical side impact is added to the input data. The full two-dimensional behavior of the pendulum is then displayed. Case 3 shows the ability of the model to produce results where intuition might fail, and the ability of the *C* code to quickly solve the fully generalized problem.

A regression procedure was developed to refine model parameters based on observed behavior. Unfortunately this procedure is not robust and frequently needs user intervention.

The model and methods presented are general and can be used for further investigations.

REFERENCES

Hindmarsh, A. C., 1983, "ODEPACK, a Systematized Collection of ODE Solvers," *Scientific Computing,* pp. 55–64.

Junkins, J. L., and Turner, J. D., 1986, *Optimal Spacecraft Rotational Maneuvers,* Elsevier, Amsterdam.

Petzold, L. R., 1983, "Automatic Selection of Methods for Solving Stiff and Nonstiff Systems of Ordinary Differential Equations," *SIAM Journal of Scientific and Statistical Computing,* Vol. 4, pp. 136–148.

Press, W. H., Flannery, B. P., Teukolsky, S. A., and Vetterling, W. T., 1989, *Numerical Recipes: The Art of Scientific Computing,* Cambridge University Press, Cambridge, UK.

Townsend, M. A., and Allan, A. P., 1994, "Poinsot's Problem: Torque-Free Rotational Dynamics of an Asymmetric Body," to appear.

Wolfram, S., 1988, *Mathematica: A System for Doing Mathematics by Computer,* Addison–Wesley, Redwood City, CA.